PHYSICAL REVIEW B **82**, 081407(R) (2010)

Transport in gapped bilayer graphene: The role of potential fluctuations

K. Zou and J. Zhu
Department of Physics, The Pennsylvania State University, University Park, Pennsylvania 16802, USA

(Received 13 July 2010; published 17 August 2010)

We employ a dual-gated geometry to control the band gap Δ in bilayer graphene and study the temperature dependence of the resistance at the charge neutrality point, $R_{NP}(T)$, from 220 to 1.5 K. Above 5 K, $R_{NP}(T)$ is dominated by two thermally activated processes in different temperature regimes and exhibits $\exp(T_3/T)^{1/3}$ below 5 K. We develop a simple model to account for the experimental observations, which highlights the crucial role of localized states produced by potential fluctuations. The high-temperature conduction is attributed to thermal activation to the mobility edge. The activation energy approaches $\Delta/2$ at large band gap. At intermediate and low temperatures, the dominant conduction mechanisms are nearest-neighbor hopping and variable-range hopping through localized states. Our systematic study provides a coherent understanding of transport in gapped bilayer graphene.

DOI: 10.1103/PhysRevB.82.081407 PACS number(s): 72.80.Vp, 73.22.Pr, 72.20.Ee

Bilayer graphene is a unique two-dimensional material with a tunable band gap. A perpendicular electric field breaks the inversion symmetry between the two graphene layers and results in a field-dependent band gap.[1–3] Its experimental signatures have been observed by infrared spectroscopy[4–7] and angle-resolved photoemission,[8] but remain incomplete and perplexing in transport.[9–12] Near room temperature, Xia *et al.*[11] observes thermally activated conduction and attributes it to Schottky barriers at the electrode-gapped bilayer interface. In the millikelvin regime, Oostinga *et al.*[10] reports variable-range hopping. To date, systematic investigations combining high and low temperatures are lacking and a coherent understanding of conduction in gapped bilayer has yet to emerge.

In this work, we control the band gap in bilayer graphene using top and bottom gates, and measure the temperature-dependent resistance at the charge neutrality point (CNP) $R_{NP}(T)$ as a function of the gap, in the temperature range of $1.5<T<220$ K. We develop a model to explain the data, which highlights the essential role of localized states produced by potential fluctuations. Our data point to three conduction mechanisms: thermal activation to the mobility edge at high temperatures, nearest-neighbor hopping (NNH) at intermediate temperatures, and variable-range hopping (VRH) at low temperatures.

We fabricate SiO_2/HfO_2 dual-gated bilayer graphene field-effect transistors using procedures previously described in Ref. 13. 30 nm HfO_2 is deposited on single or bilayer graphene by atomic layer deposition and used as the top-gate dielectrics. We have achieved high mobility μ of 9000–16 000 $cm^2/V\,s$ on single layer graphene.[13] Here, on dual-gated bilayer, μ ranges from 1500 to 6000 $cm^2/V\,s$, which is generally lower than μ up to 12 000 $cm^2/V\,s$ observed in our pristine bilayer samples. Raman spectra on dual-gated bilayer devices show no visible D band, indicating minimal defect creation (Fig. S4 in Ref. 23). The gating efficiency of the top gate is approximately $2.8\times10^{12}/cm^2$ V from Hall measurements, which is ~40 times of the efficiency of the 290 nm SiO_2 backgate. The gating range of the top gate is greater than $1.4\times10^{13}/cm^2$.

A scanning electron microscope (SEM) micrograph of a dual-gated device is shown as an inset of Fig. 1. Two types of top gates are used. In samples A1 and A2, the area between the two voltage probes is completely covered by the top-gate electrode (top of inset) so that it does not include the interfacial resistances between the gapped and ungapped area. In samples B1 and B2, the coverage is partial (bottom of inset). All four measurements yield similar behavior, indicating that the resistance of gapped bilayer is dominated by the bulk.

To obtain the T dependence of the charge neutrality point resistance $R_{NP}(T)$, we fix the backgate voltage V_{bg} and sweep the top gate V_{tg}. The sweep is repeated at different V_{bg}'s and temperatures. Figure 1 shows $R(V_{tg})$ of sample B1 at 10 K. From left to right, V_{bg} changes from +30 to −60 V at 10 V steps. The maximum resistance of each curve corresponds to the CNP for that specific pair of (V_{bg}, V_{tg}) settings. The minimum of all R_{NP} is found at roughly $V_{bg0}=0$ V and $V_{tg0}=3.1$ V in Fig. 1, which corresponds to the condition where the average band gap $\Delta=0$.[4] The offsets V_{tg0} and V_{bg0} come from unintentional chemical doping. At the CNP, Δ was shown to increase with the electric displacement field $D=D_{bg}=-D_{tg}=\epsilon_{bg}V'_{bg}/d_{bg}$, where ϵ_{bg} and d_{bg} are the dielectric constant and thickness of the backgate oxide, respectively, and $V'_{bg}=V_{bg}-V_{bg0}$ is the effective backgate

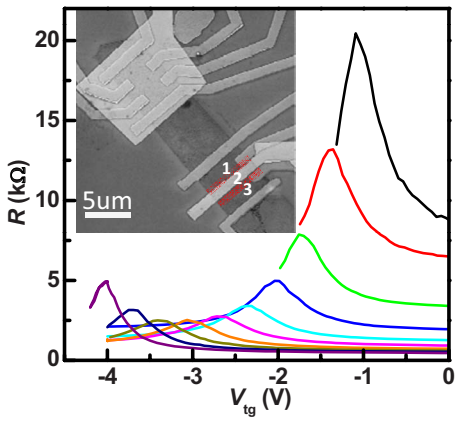

FIG. 1. (Color online) $R(V_{tg})$ at fixed V_{bg} of sample B1 at 10 K. From left to right, $V_{bg}=+30$ to −60 V at 10 V steps. Inset: a SEM picture of a device. The mobility μ is approximately 1500 $cm^2/V\,s$ for sample A1, A2 and 3000 $cm^2/V\,s$ for sample B1, B2.

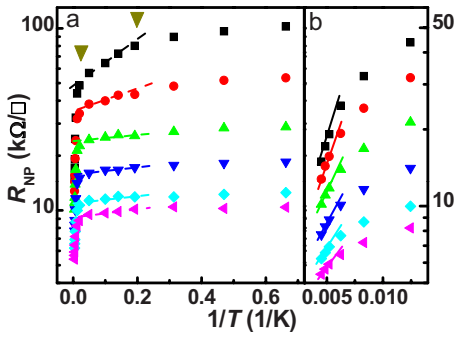

FIG. 2. (Color online) (a) $R_{NP}(T)$ of sample B1 in a semilog vs $1/T$ plot in the temperature range of $1.5<T<220$ K. From top to bottom, $V'_{bg}=-60$ to -10 V at 10 V steps. The triangles mark 50 K and 5 K, respectively. (b) The expanded region of $70<T<220$ K in (a). The solid and dashed lines in (a) and (b) are guide to the eye.

voltage.[1,4] Using $\epsilon_{SiO_2}=3.9$ and $d_{SiO_2}=290$ nm, we obtain $D=1.34$ V/nm for $V'_{bg}=100$ V. In samples B1 and B2, the resistance of the dual-gated area 2 is calculated by subtracting the resistance of areas 1 and 3 (Fig. 1 inset), which is obtained by sweeping V_{bg} while grounding V_{tg} at each temperature. Standard lock-in techniques are used with excitation current 0.2 to 50 nA. Low currents are carefully chosen for high-resistance measurements to avoid current heating.

$R_{NP}(T)$ of sample B1 is shown in a semilog vs $1/T$ plot in Fig. 2(a). From top to bottom, V'_{bg} changes from -60 to -10 V at 10 V steps. $R_{NP}(T)$ shows an insulating T dependence in the whole temperature range. The high-T region is expanded in Fig. 2(b), where log R_{NP} vs $1/T$ shows a linear trend (solid lines) at $T>150$ K. This trend suggests thermally activated conduction. From 150 to 50 K, the slopes continue to decrease, and become approximately constant again between 50 and 5 K albeit with much smaller values [dashed lines in Fig. 2(a)]. This suggests another thermally activated process with a much smaller activation energy. Below 5 K, $R_{NP}(T)$ remains nearly T independent for small $|V'_{bg}|$ and increases slowly with decreasing T for larger $|V'_{bg}|$. Similar behavior is observed on all four samples.

These observations are reminiscent of impurity conduction in doped semiconductors,[14,15] where localized states produced by impurities reside in the band tail and are separated from delocalized states by a mobility edge E_c. In such systems, thermal activation to the mobility edge dominates the high-temperature conduction. As T decreases, electrons hop through localized states, overcoming the energy difference between adjacent neighbors, i.e., nearest-neighbor hopping. At even lower T, electrons hop through localized states far from each other via the assistance of phonons of energy k_BT, giving rise to variable-range hopping.[14,15]

Localized states due to disorder also exist in bilayer graphene.[16] Scanning tunneling microscope (STM) measurements show the potential of the CNP in bilayer can fluctuate between ± 40 meV.[17] Similar observations have been made on single layers as well.[18,19] The resulting electron and hole puddles are typically a few tens of nanometers in lateral size.[17–19] In a gapped bilayer, these puddles are confined and separated from the mobility edge by a binding energy. In a zero-gap bilayer, Klein tunneling may provide a parallel conduction path to thermally activated processes.[20,21]

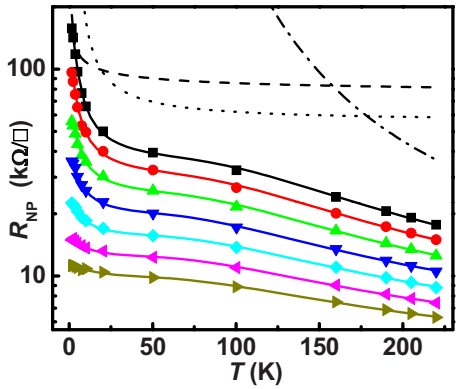

FIG. 3. (Color online) $R_{NP}(T)$ of sample A1 in the temperature range of $1.5<T<220$ K. From top to bottom, $V'_{bg}=-90$ to -30 V at 10 V steps. The solid lines are fittings to Eq. (1). The three terms in Eq. (1) are plotted as dashed-dotted, dotted, and dashed lines, respectively, for the top curve to show the contribution of each term at different temperatures.

The T dependence of $R_{NP}(T)$ in Fig. 2 and the above reasoning lead us to propose a fitting including the following three terms:

$$R_{NP}(T)^{-1}=R_1^{-1}\exp[-E_1/k_BT]+R_2^{-1}\exp[-E_2/k_BT]+R_3^{-1}\exp[-(T_3/T)^{1/3}], \quad (1)$$

where E_1, E_2 and T_3 represent the two activation energies and the hopping energy, respectively, and R_1, R_2, and R_3 are the corresponding resistance coefficients. Equation (1) produces an excellent description of $R_{NP}(T)$ in the whole temperature range in all samples. Each parameter plays a different role in the fitting.[22] The fitting curves of sample A1 are shown in Fig. 3. The combination of different energy scales accurately captures the shoulder seen around 50 K (Fig. 3), and the bend around 5 K [Fig. 2(a)] in all samples.

The extracted E_1 is plotted in Fig. 4(a) and shows similar trends in all four samples. E_1 remains approximately constant at 250 K for small $|V'_{bg}|$ (or equivalently small D), and starts to increase at larger $|V'_{bg}|$, reaching ~450 K at $V'_{bg}=-90$ V in samples A1 and A2. Also plotted in Fig. 4(a) is the calculated $\Delta/2$ of Ref. 1 (solid black line). At small $|V'_{bg}|$, E_1 differs from the small $\Delta/2$ predicted by theory but approaches theory with increasing $|V'_{bg}|$. In particular, a finite E_1 at $V'_{bg}=0$ V, where $\Delta=0$, suggests a different activation mechanism. We attribute E_1 to the activation barrier to the mobility edge, i.e., $E_1=E_c-E_F$. Since at $\Delta=0$, the Fermi level E_F lies approximately in the middle of the fluctuating disorder potential Φ, we associate $E_1=E_c$ with the root-mean-square (rms) amplitude of the potential fluctuation, i.e., $\Phi_{rms}=E_1=250$ K or 21.5 meV. Independently, Φ_{rms} in the STM data of Deshpande *et al.*[17] was found to be 19 meV,[23] in good agreement with results obtained here. In this scenario, all carriers residing in the puddles will be excited above E_c at very high temperatures. Estimating the carrier density in the puddles to be $n=\Phi_{rms}(2m^*/\pi\hbar^2)=6\times10^{11}/\text{cm}^2(m^*=0.033m_e)$ and using $\mu=1500-3000$ cm^2/V s for all samples, we expect

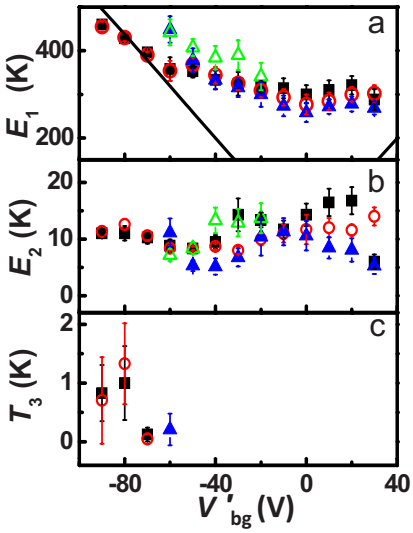

FIG. 4. (Color online) [(a)–(c)] E_1, E_2, and T_3 vs V'_{bg} for sample A1 (solid black square), A2 (hollow red circle), B1 (solid blue triangle), and B2 (hollow green triangle). The theoretical $\Delta/2$ (Ref. 1) is plotted as a solid line in (a) for comparison.

$R_1 = 1/ne\mu$ to be 3500–7000 $\Omega/\square$. R_1 extracted from the fittings ranges 3000–5000 $\Omega/\square$, in excellent agreement with our estimates.[22]

The above analysis should also hold for a small band gap $\Delta < \Phi_{rms}$, which explains the nearly flat E_1 at small $|V'_{bg}|$ in Fig. 4(a). As Δ further increases, we expect E_1 to be gradually dominated by the band gap itself and eventually approach $\Delta/2$. Our results in Fig. 4(a) support this trend. The above model also explains the insulating T dependence widely observed near the CNP in backgated bilayers.[24–27]

As T decreases, the above thermally activated conduction becomes inefficient; our data in Fig. 2 show that other low-energy processes gradually take over from 150 to 50 K. Between $50 > T > 5$ K, the rise of $R_{NP}(T)$ is largely given by the second exponential term in Eq. (1) (Fig. 3). The extracted activation energy E_2 is shown in Fig. 4(b). E_2 is nearly V'_{bg} independent and averages ~10 K, or 25–50 times smaller than E_1, in all samples. In doped semiconductors, E_2 is associated with the hopping conduction between nearest-neighboring impurity states. In percolation theory, $E_2 = \langle \varepsilon_{ij} \rangle = \langle \varepsilon_i - \varepsilon_j \rangle$ is the average energy difference between neighboring localized states on the percolation path.[14] Similar to the localized states in doped semiconductors, in a gapped bilayer, electron and hole states near the band edges are quantized and localized due to small puddle size.[28] These localized states may support a hopping conduction that is more effective than the thermal activation above the mobility edge at $k_B T \ll E_1$. In this scenario, the hopping is expected to occur between nearest neighbors when the temperature is not too low and transitions to VRH at the lowest temperatures.[14] These two hopping processes can account for the $\exp[-E_2/k_B T]$ and the $\exp[-(T_3/T)^{1/3}]$ terms necessary to describe our data.

The following analysis provides an order of magnitude estimate of $E_2 = \langle \varepsilon_{ij} \rangle$ in our samples. We assume the distribution of the puddle size L in our samples is similar to that in Ref. 17, since both samples are on SiO_2 substrates and have similar Φ_{rms}. This distribution is estimated by analyzing the potential map of the CNP in Ref. 17. A histogram of L is generated and modeled by a Gaussian distribution as shown in Fig. S2(b).[23] The best fit yields $L = (13 \pm 8.4)$ nm, consistent with other STM reports.[19] In our simplified model, the disorder potential Φ is approximated by a random network of cylindrical wells with a single depth V_0 but varying diameter L as shown in Fig. 5(a), neglecting the shape variation and the distribution of V_0. The bound-state energy ε_i of each well is calculated using a constant effective mass $m^* = 0.033 m_e$.[29] Figure 5(b) plots ε_i vs L for two representative V_0's. The solid curve corresponds to $V_0 = 43$ meV, which is $2\Phi_{rms}$ in our samples. The dashed curve corresponds to $V_0 = 13$ meV. We obtain the average $\langle \varepsilon_{ij} \rangle$ using $\varepsilon_i(L)$ and the distribution of L,[23] including puddles of all sizes.[30] We find $\langle \varepsilon_{ij} \rangle = 110$ K and 9 K for $V_0 = 43$ meV and 13 meV, respectively. In real samples V_0 obeys a Gaussian distribution.[23] Statistically 25% of all puddles have $V_0 < 13$ meV and 68% of all puddles obey $V_0 < 43$ meV. Thus these calculations provide reasonable bounds for $\langle \varepsilon_{ij} \rangle$ in our samples. The above analysis suggests that $\langle \varepsilon_{ij} \rangle$ is likely to be a few tens of kelvin, which is in reasonable agreement with our extracted $E_2 \approx 10$ K and supports the NNH scenario.

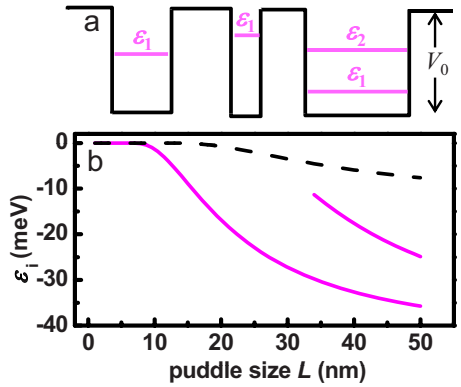

FIG. 5. (Color online) (a) A simple model of the potential fluctuations in bilayer. The bound state of each cylindrical well is schematically shown. A wide well may have more than one bound state. (b)The bound-state energy $\varepsilon_i(L)$ for $V_0 = 43$ meV (solid magenta line) and $V_0 = 13$ meV (dashed black line).

The above model points to the onset of VRH conduction at yet lower temperature. Indeed, $R_{NP}(T)$ data in Fig. 2(a) shows a bend at 5 K. We have verified that this bend is not due to current heating. Although the temperature range is limited, the VRH term in Eq. (1) is necessary to capture this behavior. At large $|V'_{bg}|$, the extracted T_3 ranges 0.7–1.3 K as shown in Fig. 4(c). These values are in very good agreement with $T_3 = 0.5$–0.8 K obtained in Ref. 10, where the VRH conduction is observed in similar samples for a larger temperature range $5\ \text{K} > T > 50$ mK. At small $|V'_{bg}|$, T_3 is so small that $R_{NP}(T)$ remains essentially T independent, probably due to Klein tunneling.

The corresponding R_3 is ~8 k$\Omega/\square$ at small $|V'_{bg}|$ and increases with increasing $|V'_{bg}|$ in all samples. R_3 reaches approximately 75 k$\Omega/\square$ in samples A1 and A2 at $|V'_{bg}| = 90$ V. This trend is consistent with the increasing sup-

pression of Klein tunneling as Δ increases. The opening of the gap may also alter the strength of the electron-acoustic phonon coupling, which is essential to the VRH process, and affect R_3. As a final check, we note that VRH is expected to occur at $T \ll T_c$, where T_c is determined by Eq. (2), where the variable activation energy E_a becomes roughly 1/3 of E_2,[14]

$$E_a(T_c) = \left.\frac{d(\ln R)}{d(k_B T)^{-1}}\right|_{T=T_c} = \frac{k_B T_3^{1/3} T_c^{2/3}}{3} \approx \frac{E_2}{3}. \qquad (2)$$

Using $T_3=0.9$ K and $E_2=10$ K, we obtain $T_c=33$ K. Thus, the assignment of VRH at $T<5$ K is self-consistent.

In conclusion, we measure the T-dependent resistance at the charge neutrality point in gapped bilayer and develop a simple model to account for the observed multiple energy scales. Localized states produced by potential fluctuations play a crucial role in our model. At high temperatures, thermal activation to the mobility edge dominates the conduction. The activation energy is determined by the potential fluctuations at small band gap and approaches that of a band insulator at large band gap or in clean samples. At lower temperatures, a percolation network forms via carrier hopping through localized states, leading to a second activated process and eventually variable-range hopping. Our model provides important insights into electrical transport in gapped bilayer graphene, which may be useful in a range of electronic and optical applications.

Note added in proof. Recently, we became aware of two related works.[31,32]

We thank Brian LeRoy for sharing his STM data with us. We are grateful for a stimulating discussion with Pablo Jarillo-Herrero and thank Vin Crespi and Jainendra Jain for useful comments. This work is supported by NSF CAREER under Grant No. DMR-0748604 and NSF NIRT under Grant No. ECS-0609243. The authors acknowledge use of facilities at the PSU site of NSF NNIN.

[1] E. McCann, Phys. Rev. B **74**, 161403 (2006).
[2] H. Min, B. Sahu, S. K. Banerjee, and A. H. MacDonald, Phys. Rev. B **75**, 155115 (2007).
[3] P. Gava, M. Lazzeri, A. M. Saitta, and F. Mauri, Phys. Rev. B **79**, 165431 (2009).
[4] Y. B. Zhang, T. T. Tang, C. Girit, Z. Hao, M. C. Martin, A. Zettl, M. F. Crommie, Y. R. Shen, and F. Wang, Nature (London) **459**, 820 (2009).
[5] K. F. Mak, C. H. Lui, J. Shan, and T. F. Heinz, Phys. Rev. Lett. **102**, 256405 (2009).
[6] A. B. Kuzmenko, E. van Heumen, D. van der Marel, P. Lerch, P. Blake, K. S. Novoselov, and A. K. Geim, Phys. Rev. B **79**, 115441 (2009).
[7] L. M. Zhang, Z. Q. Li, D. N. Basov, M. M. Fogler, Z. Hao, and M. C. Martin, Phys. Rev. B **78**, 235408 (2008).
[8] T. Ohta, A. Bostwick, T. Seyller, K. Horn, and E. Rotenberg, Science **313**, 951 (2006).
[9] E. V. Castro, K. S. Novoselov, S. V. Morozov, N. M. R. Peres, J. M. B. Lopes dos Santos, J. Nilsson, F. Guinea, A. K. Geim, and A. H. Castro Neto, Phys. Rev. Lett. **99**, 216802 (2007).
[10] J. B. Oostinga, H. B. Heersche, X. L. Liu, A. F. Morpurgo, and L. M. K. Vandersypen, Nature Mater. **7**, 151 (2008).
[11] F. N. Xia, D. B. Farmer, Y. M. Lin, and P. Avouris, Nano Lett. **10**, 715 (2010).
[12] S. Kim and E. Tutuc, arXiv:0909.2288 (unpublished).
[13] K. Zou, X. Hong, D. Keefer, and J. Zhu, arXiv:0912.1378 (unpublished).
[14] B. I. Shklovskii and A. L. Efros, *Electronic Properties of Doped Semiconductors* (Springer, New York, 1984).
[15] N. F. Mott, *Conduction in Non-Crystalline Materials* (Oxford University Press, New York, 1993).
[16] J. Nilsson and A. H. Castro Neto, Phys. Rev. Lett. **98**, 126801 (2007).
[17] A. Deshpande, W. Bao, Z. Zhao, C. N. Lau, and B. J. LeRoy, Appl. Phys. Lett. **95**, 243502 (2009).
[18] J. Martin, N. Akerman, G. Ulbricht, T. Lohmann, J. H. Smet, K. Von Klitzing, and A. Yacoby, Nat. Phys. **4**, 144 (2008).
[19] Y. B. Zhang, V. W. Brar, C. Girit, A. Zettl, and M. F. Crommie, Nat. Phys. **5**, 722 (2009).
[20] M. I. Katsnelson, K. S. Novoselov, and A. K. Geim, Nat. Phys. **2**, 620 (2006).
[21] E. Rossi, J. H. Bardarson, P. W. Brouwer, and S. Das Sarma, Phys. Rev. B **81**, 121408 (2010).
[22] The only ambiguous fitting cases are with the determination of E_1 and R_1 in samples A1 and A2 for $V'_{bg}=-70$, -80, and -90 V. There, E_1 and R_1 show strong correlations. We have fixed $R_1=4500$ Ω based on results at smaller $|V'_{bg}|$ and determined E_1 accordingly.
[23] See supplementary material at http://link.aps.org/supplemental/10.1103/PhysRevB.82.081407 for Raman and analysis of puddles.
[24] S. V. Morozov, K. S. Novoselov, M. I. Katsnelson, F. Schedin, D. C. Elias, J. A. Jaszczak, and A. K. Geim, Phys. Rev. Lett. **100**, 016602 (2008).
[25] B. E. Feldman, J. Martin, and A. Yacoby, Nat. Phys. **5**, 889 (2009).
[26] K. Zou, X. Hong, and J. Zhu (unpublished).
[27] E. Hwang and S. Das Sarma, arXiv:1006.1897 (unpublished).
[28] The states are localized when the band gap is sufficiently large so that the puddles are separated by tunnel barriers. When the gap is small, Klein tunneling should take place although calculations show that it may be suppressed by strong disorder (Ref. 21). Experimentally, the weak T dependence of $R_{NP}(T)$ at low V'_{bg} renders the distinction of the second and third term in Eq. (1) less meaningful. These subtleties should be kept in mind when looking at E_2 extracted for small V'_{bg}.
[29] Reference 3 predicts a much larger m^* near the CNP in gapped bilayer. A heavier mass means lower ε_i and more bound states in a well, which may lead to lower $\langle \varepsilon_{ij} \rangle$. This effect has not been included in our simulations.
[30] Puddles on the percolation path may have a narrower energy distribution and consequently lower $\langle \varepsilon_{ij} \rangle$. This effect has not been considered in our simulations.
[31] J. Yan and M. S. Fuhrer (unpublished).
[32] L. Jing, J. Velasco Jr., P. Kratz, G. Liu, W. Bao, M. Bockrath, and C. N. Lau (unpublished).